TRANSACTIONS ON ELECTRICAL AND ELECTRONIC MATERIALS
Vol. 16, No. 4, pp. 194-197, August 25, 2015

Regular Paper

pISSN: 1229-7607 eISSN: 2092-7592
DOI: http://dx.doi.org/10.4313/TEEM.2015.16.4.194
OAK Central: http://central.oak.go.kr

Characteristics of Lanthanum Silicates Electrolyte for Solid Oxide Fuel Cells

Dong-Jin Lee, Sung-Gap Lee†, Hyun-Ji Noh, and Ye-Won Jo
Department of Ceramic Engineering, RIGET, Gyeongsang National University, Jinju 660-701, Korea

Received June 8, 2015; Revised July 13, 2015; Accepted July 18, 2015

$La_{9.33}(Si_5V_1)O_{26}$ ceramics were fabricated by the mixed oxide method for solid oxide electrolytes. $La_{9.33}(Si_5V_1)O_{26}$ specimens showed the hexagonal, space group P63 or P63/m, and the unit cell volume increased when the sintering temperature increased. The specimen sintered at 1,400℃ showed the X-ray patterns of the homogeneous apatite single phase without the second phase, such as La_2SiO_5 and SiO_2. The specimen sintered at 1,400℃ showed the maximum sintered density of 4.93 g/cm^3. When the sintering temperature increased, the electrical conductivities increased, the activation energy decreased and the values were 7.83×10^{-4} S/cm, 1.61 eV at 600℃, respectively.

Keywords: SOFC, Lanthanum silicate, La9.33$(Si_5V_1)O_{26}$, Mixed-oxide method

1. INTRODUCTION

Solid electrolyte fuel cells or solid oxide fuel cells (SOFC), which is a fuel cell using the ion conductor, is the effective energy conversion mechanism that directly converts chemical energy into electrical energy. Because of the high power generation efficiency of the conventional heat engine, the ability to operate it at a high temperature and the potential for combining heat within the power plant, small-scale distributed power between the power supply, the thermal power plants and large-scale commercialization are possible. On the other hand, solar, green energy, such as a bio-energy, and wind energy, has attracted much interest to solve the energy shortage problem due to the exhaustion of fossil fuel and the environmental problems caused by the use of fossil fuels. In particular, a solid electrolyte fuel cell using hydrogen as a fuel has recently been studied. In general, the solid electrolyte used the ion conduction mechanism according to the oxygen vacancies that are generated by the addition of impurities to the basic compositions of the zirconia materials that have a fluorite structure and the La-SrO-GaO-MgO (LSGM) perovskite structure [1-5].

On the other hand, the silicate apatite materials based on the rare earth metals are known to have an interstitial oxygen ion conductive mechanism with a c-axis preferred orientation [7-9]. Therefore, the apatite materials are considered as a new electrolyte material that has excellent ion conductivity at a low operating temperature. In addition, the rare earth metal-based apatite materials, such as $La_{9.33}(Si_5V_1)O_{26}$, have the following properties: a high sintering temperature of about 1,600℃ and an improving ion conductivity with an increased cation radius [10-12]. In this study, the V element that has a low melting temperature was added to the $La_{9.33}(Si_5V_1)O_{26}$ materials, which have good electrical conductivity properties in the middle and low temperature region. The V element was added to address the high sintering temperature and to increase the ion conductivity property in the rare earth metal-based apatite material. In addition, their structural and electrical properties were investigated for the solid oxide fuel cell.

2. EXPERIMENT

La_2O_3(99%), SiO_2(99%) and V2O5(99%) were used as the starting materials according to the composition formula $La_{9.33}(Si_5V_1)O_{26}$. La_2O_3 powder, which easily reacts with moisture in the air, was heated for 2 hours at 1,100℃ before it was weighed. Then, the raw materials were mixed and ground in ethylalcohol using

† Author to whom all correspondence should be addressed:
E-mail: lsgap@gsnu.ac.kr

a zirconia ball for 24 hours. Subsequently, the mixed powder was calcined in air at 1,200℃ for 2 hours and mixed with the organic binder of 3 wt% PVA. After being dried, the powder was pressed under a hydrostatic pressure of 150 MPa to be a pellet, followed by sintering at 1,300~1,450℃ for 2 hours in air. Structural properties of the specimens were measured by X-ray powder diffraction with an X-ray powder diffractometer filtered CuKα radiation at 40 kB acceleration voltage and 30 mA tube current. The AC electrical properties, such as electrical conductivity and activation energy, were measured using a multi-frequency LCR meter (Fluke PM 6306) in the frequency range of 60 Hz to 1 MHz.

3. RESULTS AND DISCUSSION

Figure 1 shows the X-ray diffraction patterns of the $La_{9.33}(Si_5V_1)O_{26}$ specimens as a function of the sintering temperature. The diffraction patterns of all specimens were almost the same as the basic composition of lanthanum silicate. In the specimens sintered at 1,350℃ and 1,450℃, the second phase, such as La_2SiO_5 and SiO_2, were observed and the specimen sintered at 1,400℃ showed the homogeneous X-ray diffraction pattern of the single apatite phase without the second phase.

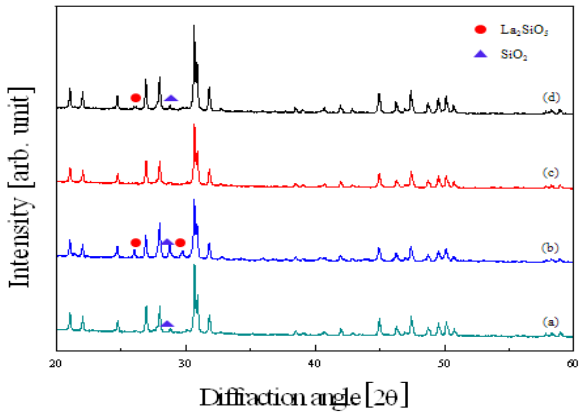

Fig. 1. X-ray diffraction patterns of $La_{9.33}(Si_5V_1)O_{26}$ ceramics as a function of sintering temperatures: (a) 1,300℃, (b) 1,350℃, (c) 1,400℃, and (d) 1,450℃.

Table 1 shows the crystallographic properties of the $La_{9.33}(Si_5V_1)O_{26}$ specimens as a function of the sintering temperature. $La_{9.33}(Si_5V_1)O_{26}$ specimens are sintered at 1,600℃ generally. However, $La_{9.33}(Si_5V_1)O_{26}$ specimens added to V element were sintered well at about 1,400℃. This property is due to the addition of V element that has a low melting temperature. In addition, a unit volume and the lattice constant were increased as the sintering temperature increased because the larger ionic radius of V (0.58 Å) is substituted for Si (0.39 Å) position.

Figure 2 shows the sintered density of the $La_{9.33}(Si_5V_1)O_{26}$ specimens as a function of the sintering temperature. The sintered density increased when the sintering temperature increased. However, the specimens sintered at a temperature higher than 1,400℃ exhibited saturation characteristics. This phenomenon may result from decreasing the pore size and increasing the grain size as the sintering temperature increases, and the grain growth and the vacancy of V ions coexist due to the high sintering temperature when the sintering temperature is higher than 1,400℃.

Figure 3 shows the surface and cross-sectional scanning electron microscope (SEM) images of the $La_{9.33}(Si_5V_1)O_{26}$ specimens as a function of the sintering temperature. As the sintering temperature increases, a dense microstructure is exhibited due to a decrease in the porosity and an increase in the grain size because some V ions, which have a low melting point, are deposited at grain boundaries, which promote grain growth. The specimen sintered at 1,400℃ showed a dense microstructure. Microstructure characteristics, such as the sintering temperature, tended to match the sintered density properties, as shown in Fig. 2.

Table. 1. Crystalline properties of apatite $La_{9.33}(SiO_4)_4O_2$ and $La_{9.33}(Si_5V_1)O_{26}$ ceramics.

Composition	Sintering temperature	Space group	Unit cell parameters		
			a(nm)	C(nm)	Cell volume
$La_{9.33}(SiO_4)_6O_2$	1,600℃	$P6_3/m$	9.725	7.1850	588.52
$La_{9.33}(Si_5O_1)O_{26}$	1,300℃	$P6_3/m$	9.729	7.183	589.40
$La_{9.33}(Si_5O_1)O_{26}$	1,350℃	$P6_3/m$	9.732	7.196	590.25
$La_{9.33}(Si_5O_1)O_{26}$	1,400℃	$P6_3/m$	9.734	7.197	590.56
$La_{9.33}(Si_5O_1)O_{26}$	1,450℃	$P6_3/m$	9.736	7.198	590.89

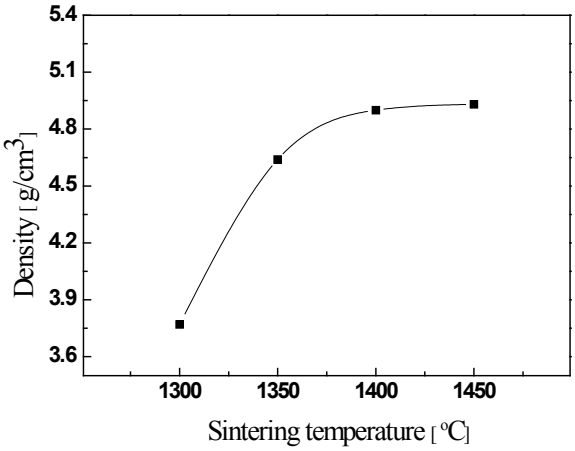

Fig. 2. Sintered density of $La_{9.33}(Si_5V_1)O_{26}$ ceramics as a function of sintering temperatures.

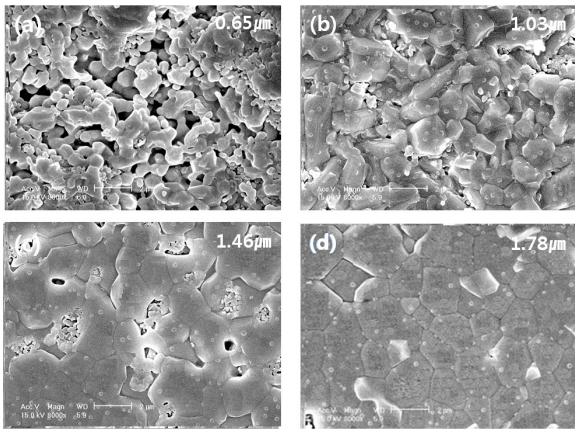

Fig. 3. SEM surface images of $La_{9.33}(Si_5V_1)O_{26}$ ceramics as a function of sintering temperatures: (a) 1,300℃, (b) 1,350℃, (c) 1,400℃, and (d) 1,450℃.

Figure 4 shows the Energy Dispersive X-ray (EDX) analysis of the $La_{9.33}(Si_5V_1)O_{26}$ specimens as a function of the sintering temperature. The ratio of V ions decreased as the sintering temperature in all specimens increased because the volatilization of V ions increased as the sintering temperature increased.

Figure 5 shows the complex impedance of the $La_{9.33}(Si_5V_1)O_{26}$

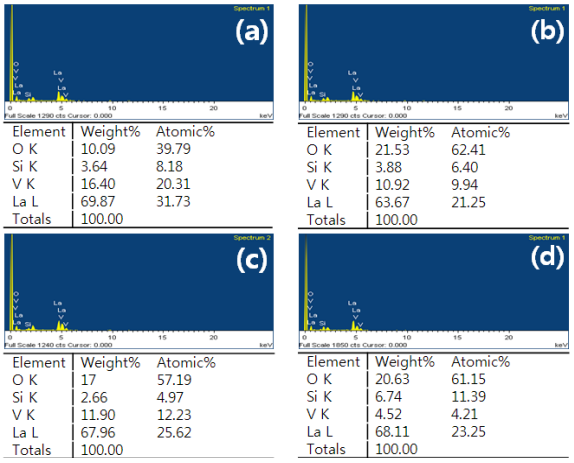

Fig. 4. EDX analysis of $La_{9.33}(Si_5V_1)O_{26}$ ceramics as a function of sintering temperatures: (a) 1,300℃, (b) 1,350℃, (c) 1,400℃, and (d) 1,450℃.

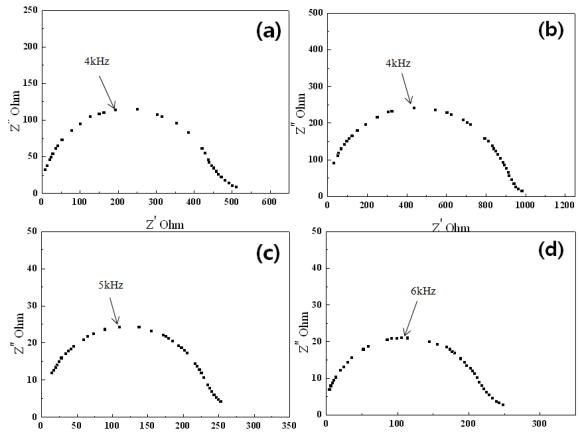

Fig. 5. Impedance plots (Z' and Z'') obtained at 600℃ of $La_{9.33}(Si_5V_1)O_{26}$ specimens as a function of sintering temperatures: (a) 1,300℃, (b) 1,350℃, (c) 1,400℃, and (d) 1,450℃.

specimens as a function of the sintering temperature, measured at 600℃. In general, the maximum impedance of the grain phase is reported to appear in a frequency of a few hundred kHz or higher [13]. However, in this study, the maximum impedance has been observed in the region of several kHz of the grain boundary characteristics, because the resistance of the grains is very small relative to the resistance of the grain boundaries. Brailsford and Hohnke [14] reported that in the complex impedance spectrum of the dielectric materials, the semi-circle spectrum represented the grain boundary, which expanded while maintaining its shape as the porosity increased. Therefore, the increasing porosity caused by the volatilization of V ions that has a low melting temperature is expected to lead to an increase in the grain boundary resistance. When increasing the sintering temperature, the electrical resistance of the specimen decreased due to a decrease in porosity and increase in the grain size.

Figure 6 shows the ionic conductivity of the $La_{9.33}(Si_5V_1)O_{26}$ specimen as a function of the sintering temperature, measured at 600℃. Ionic conductivity showed the highest value of 7.83×10^{-3} S/cm in the specimen sintered at 1,400℃, and tended to decrease gradually as the sintering temperature increased. This is thought to be due to the ionic conductivity based on the grain growth and the porosity that decreases as the sintering temperature increases. However, the conductivity of the specimen sintered at more than 1,450℃ decreased slightly decreased due to the volatile of V ions.

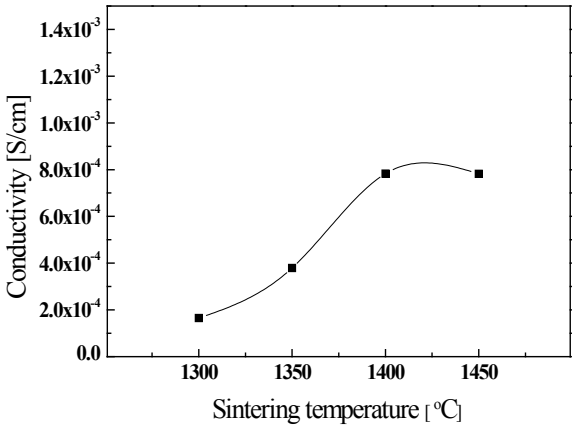

Fig. 6. Conductivity of $La_{9.33}(Si_5V_1)O_{26}$ ceramics as a function of the sintering temperature.

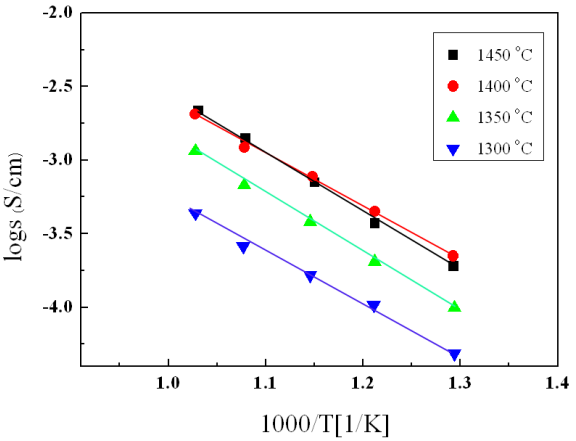

Fig. 7. Arrhenius plots of the electrical conductivity of $La_{9.33}(Si_5V_1)O_{26}$ ceramics.

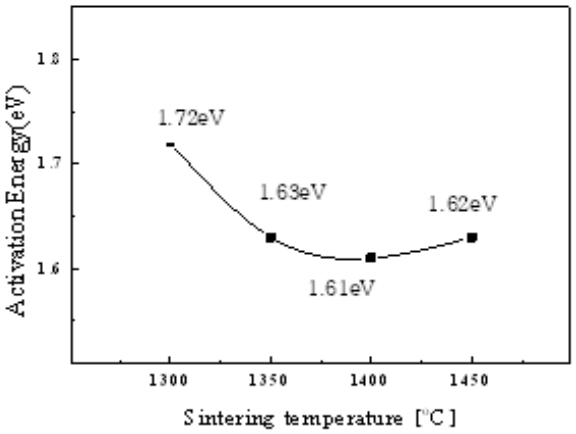

Fig. 8. Activation energy of $La_{9.33}(Si_5V_1)O_{26}$ ceramics as a function of sintering temperatures.

Figure 7 shows the Arrhenius plot of the $La_{9.33}(Si_5V_1)O_{26}$ specimens as a function of the sintering temperature. In all specimens, the ion conductivity increased with an increase in the sintering temperature. In addition, the activation energy could

be obtained by the slope of that characteristic [14,15].

Figure 8 shows the activation energy of the $La_{9.33}(Si_5V_1)O_{26}$ specimen as a function of the sintering temperature. The specimen sintered at 1,400℃ showed the lowest value of 1.61 eV. However, the theoretical value of the activation energy by interstitial conduction and oxygen vacancy conduction are 0.56 eV and 1.23 eV, respectively [16].

4. CONCLUSIONS

In this study, $La_{9.33}(Si_5V_1)O_{26}$ specimens with the apatite structure were fabricated using a mixed oxide method for the solid electrolyte fuel cells, and the structural and electrical properties were investigated according to the sintering temperature. The specimen sintered at 1,400℃ exhibited the X-ray diffraction pattern that has a homogeneous and single apatite phase. As the sintering temperature increases, the sintered density increased due to an increase in the driving force of the liquid phase sintering. However, for the specimen sintered at more than 1,450℃, the sintering density did not increase because of the compensating effect of the increased grain size and pores that was due to the volatilization of the V ion. The electrical resistance increased when the sintering temperature increased, and the complex impedance predominantly exhibited grain boundary resistance characteristics. Ion conductivity and activation energy of the specimen sintered at 1,400℃, measured at 600℃, were 7.83×10^{-4} S/cm and 1.61 eV, respectively.

REFERENCES

[1] H. Arikawa, H. Nishiguchi, T. Ishihara, and Y. Takita, Solid State Ionics, 136, 31 (2000). [DOI: http://dx.doi.org/10.1016/S0167-2738(00)00386-6]

[2] X. Zhang, S. Ohara, R. Maric, H, OKawa, T. Fukui, H. Yoshida, T. Inagaki, and K. Miura, Solid State Ionics, 133, 153 (2000). [DOI: http://dx.doi.org/10.1016/S0167-2738(00)00744-X]

[3] M. Hrovat, A. Ahmad-Khanlou, Z. Samarzija, and J. Hole, Mater. Res. Bull., 34, 2027 (1999). [DOI: http://dx.doi.org/10.1016/S0025-5408(99)00220-2]

[4] E. Djurado and M. Labeau, J. Anal. Chem., 365, 277 (1999). [DOI: http://dx.doi.org/10.1007/s002160051488]

[5] J. S. Lee, M. Lerch, J. Maier, J. Solid State Chemistry, 179, 270 (2006). [DOI: http://dx.doi.org/10.1016/j.jssc.2005.10.012]

[6] H. Yoshioka, J. Am. Ceram. Soc., 90, 3099 (2007). [DOI: http://dx.doi.org/10.1111/j.1551-2916.2007.01862.x]

[7] E. Kendrick, M. Islam, and P. Slater, J. Mater. Chem., 17, 3104 (2007). [DOI: http://dx.doi.org/10.1039/b704426g]

[8] J. R. Tolchard, M. S. Islam, and P. R. Slater, J. Mater. Chem., 12, 1956 (2005).

[9] G. Blasse, J. Solid State Chem., 12, 181 (1975). [DOI: http://dx.doi.org/10.1016/0022-4596(75)90009-2]

[10] S. C. Singhal and K. Kendall, High temperature Solid Oxide Fuel Cells: Fundamentals, Design and Applications (Elsevier, Oxford, UK, 2003).

[11] S. Nakayma, T. Kageyama, H. Aono, Y. J. Sadaoka, Mater. Chem., 5, 1801 (1995). [DOI: http://dx.doi.org/10.1039/jm9950501801]

[12] S. Shin, H. H. Huang, and M. Ishigame, Solid State Ionics, 40, 910 (1990). [DOI: http://dx.doi.org/10.1016/0167-2738(90)90151-G]

[13] A. D. Brailsford and D. K Hohnke, Solid State Ionics, 11, 133 (1983). [DOI: http://dx.doi.org/10.1016/0167-2738(83)90050-4]

[14] R. A. Alberty and R. J. Silbey, Physical Chemistry (New York, Wiley, 1997).

[15] W. Stiller, Arrhenius Equation and non-equilibrium kinetics: 100 years Arrhenius Equation. Leipzig, BSB B.G. Teubner, (1989)

[16] K. D. Kruer and Ann, Rev. Mater. Res., 33, 333 (2003). [DOI: http://dx.doi.org/10.1146/annurev.matsci.33.022802.091825]